ROYAL SOCIETY OF CHEMISTRY

PAPER

Check for updates

Sensitivity of ice nucleation parameterizations to the variability in underlying ice nucleation rate coefficients

Isabelle Steinke [ID] * and Susannah M. Burrows [ID]

Deriving aerosol-type-dependent parameterizations for ice nucleation processes remains challenging due to large uncertainties associated with laboratory studies and field measurements. One source of uncertainty is a lack of knowledge about the magnitude of particle-to-particle differences in freezing efficiency associated with particles' chemical composition and surface features. In most experimental setups, it is challenging to disentangle the contributions of inherent experimental uncertainties, variability in aerosol surface area and the particle-to-particle differences in freezing efficiency. Therefore, in this study, we use a Monte Carlo approach to simulate synthetic ice nucleation experiments to better understand the impact of variability in heterogeneous ice nucleation propensities on simulated frozen fractions. We represent this variability by differently-shaped distributions of the heterogeneous ice nucleation rate coefficients J_{het}. Distributions spanning one order of magnitude result in simulated median frozen fractions that are up to a factor of two higher compared to simulations with narrow Gaussian distributions, in the case of small frozen fractions. For the assumed range of variability in J_{het}, impacts on cloud variables (*e.g.*, ice water path based on Hawker *et al.* (2021)) calculated from hypothetical parameterizations based on our simulated frozen fractions seem to be relatively small, with only up to 25% difference between lognormal and constant J_{het} distributions. One of the major unknowns, however, is the interparticle variability in J_{het}, which depends on particle composition and surface features. Resolving this uncertainty requires a combination of laboratory studies and field experiments relating physicochemical particle features and ice nucleation propensity in a size-resolved manner.

Environmental significance

The representation of cloud ice formation remains one of the largest uncertainties in climate models, with ice nucleation parameterizations representing primary ice formation in clouds being a major contributor to this uncertainty. As of now, these parameterizations do not account for the particle-to-particle variability of ice nucleation propensities in a systematic manner. Based on our simulations of freezing droplet ensembles, the variability in ice nucleation propensities is mostly relevant at small frozen fractions and for polydisperse aerosol populations. Estimates of cloud impacts based on our simulations indicate only a minor influence of the particle-to-particle variability of ice nucleation propensities. However, these effects could be significantly larger for mixtures of particle types with dramatically different ice nucleation propensities.

1 Introduction

The cloud ice phase has a defining impact on the formation of precipitation and the atmospheric radiation budget.[1,2] However, the representation of cloud ice formation processes in weather prediction and climate models is challenging, limiting our ability to predict cloud phase and climate feedbacks.[3,4] Representing cloud formation processes and associated climate impacts in Earth system models requires the development of parameterizations that reliably predict ice crystal concentrations for complex ambient particle populations present at cloud altitude. Ambient particles are characterized by a wide range of particle sizes, compositions, and surface properties, and their ice nucleation propensities may therefore vary by several orders of magnitude.[5]

Additional challenges for predicting cloud phase include representing particle emissions and other processes that control the atmospheric population of particles participating in ice nucleation.[6] Further complexity is introduced by processes controlling the cloud response to ice-nucleating particles (INPs), including secondary ice formation processes,[7] and the multiscale interactions between cloud microphysical and dynamical processes.[8] Improved prediction of the cloud phase and its response to Earth system processes will ultimately require improvements to the predictability of both INPs and cloud responses.[9]

Atmospheric Sciences & Global Change Division, Pacific Northwest National Laboratory, Richland, Washington, USA. E-mail: isabelle.steinke@pnnl.gov

© 2022 The Author(s). Published by the Royal Society of Chemistry

Environ. Sci.: Atmos., 2022, **2**, 1101–1107 | 1101

In this study, we focus our discussion on parameterizations describing immersion freezing (*i.e.*, the formation of ice crystals in cloud droplets), which is the primary pathway for heterogeneous ice nucleation in mixed-phase clouds.[10] Recently, aerosol-type-dependent ice nucleation propensities have been characterized by either ice nucleation active surface site (INAS) densities or heterogeneous nucleation rate coefficients. These approaches differ in their treatment of the observed time dependence, describing the frozen fraction f_{ice} by

$$f_{ice} = 1 - \exp(-J_{het}(T)At) \tag{1}$$

and

$$f_{ice} = 1 - \exp(-n_s(T)A) \tag{2}$$

where J_{het} is the heterogeneous nucleation rate coefficient, n_s is the INAS density, A is the aerosol surface area available for ice nucleation, and t is the time that has passed since the start of the nucleation event. For immersion freezing, J_{het} and n_s are temperature (T) dependent. Eqn (1) and (2) can be interpreted as the median freezing curves for a sufficiently large droplet ensemble and a chemically homogeneous particle population.[11]

Several approaches have been used to expand the applicability of eqn (1) and (2) by accounting for the variability in A and J_{het}/n_s. Instead of using a single value to represent aerosol-type-dependent ice nucleation propensities (J_{het}, n_s), distributions of values have been found to better represent ice nucleation propensities observed for certain particle types, *e.g.*, mineral dust.[12–15] This heterogeneity in ice nucleation propensities is caused by variations in particle composition and morphology, which are highly variable across aerosol particle classes and even within populations of a similar particle type.[5,16,17] Note that in some cases, ice nucleation propensities and their variabilities are also expressed as more indirectly derived metrics, *e.g.*, as contact angles.[14,18,19] Most approaches accounting for the heterogeneity of ice nucleation propensities implicitly assume that the relevant quantity describing the observed ice nucleation efficiency (*e.g.*, contact angle θ) follows a Gaussian distribution.[18,20,21] However, it is not clear *a priori* which distribution shapes are most suitable for representing the ice nucleation behavior of complex ambient particles. Also, most studies implicitly assume that the ensemble of freezing droplets or aliquots is large[11] and therefore neglect stochastic uncertainties.[22] For the aerosol surface area (A), which is an important quantity in ice nucleation studies, observed size distributions are commonly approximated by lognormal distributions.[23,24]

In this study, we use Monte Carlo simulations to conduct synthetic ice nucleation experiments, with the goal to better understand the interplay between aerosol size distributions, J_{het} distribution shapes, and droplet ensemble sizes in determining the range of observable frozen fractions in ice nucleation experiments.

2 Methods

Synthetic experimental data are commonly used to better understand the causes of features observed in laboratory and field experiments, *e.g.*, to analyze orographic effects on precipitation (Bae and Oh[25]), to better understand the performance of cloud probes,[26] or to evaluate methane emissions.[27] Here, we use synthetic experiments to test the impact of different particle characteristics (size distributions, temperature-dependent ice nucleation efficiencies) on simulated frozen fractions while using these simulations to mimic the characteristics of real-world experimental setups (*e.g.*, droplet ensemble sizes).

2.1 General setup of Monte Carlo simulations

We simulate two different types of droplet ensembles: ensembles with relatively few freezing droplets ($N_{drop} = 100$) and ensembles with many freezing droplets ($N_{drop} = 10\,000$). Smaller droplet ensembles ($N_{drop} < 100$) can be found for droplet freezing assays that investigate the freezing of suspension droplets, whereas the latter ensemble type is more representative of continuous flow diffusion chamber (CFDC) experiments.[28] In the context of ambient INP measurements, droplet freezing experiments are commonly used to analyze previously collected samples for ice nucleation activity at warmer temperatures (*e.g.*, >−25 °C), while CFDC experiments produce real-time measurements of INP concentrations (typically at $T < -20$ °C).[5,17]

For an ensemble of droplets, we describe the freezing behavior of an individual freezing droplet (j) containing a particle with surface A_j by

$$P_{j,frz} = 1 - \exp(-J_{het,j} \cdot A_j \cdot \delta t). \tag{3}$$

We introduce the element of stochasticity by evaluating freezing probabilities against a random number between 0 and 1, and simulate a freezing event when that random number exceeds $P_{j,frz}$, following the procedure described in Alpert and Knopf (2016).[22] All values for $J_{het,j}$ and A_j are sampled from distributions described in the following sections. For simplicity, we evaluate frozen fractions after $\delta t = 10$ s, assuming that the temperature remains constant during the simulated time interval. The value chosen for time scale δt corresponds to the order-of-magnitude residence time within most current CFDC-style experiments.[28] For each droplet freezing ensemble, we conduct 100 000 simulation runs.

2.2 Simulated ice nucleation rate coefficient distributions

Through our synthetic experiments, we analyze the range of possible outcomes (*i.e.*, the stochastic uncertainty associated with simulated frozen fractions), depending on the shape and width of the underlying J_{het} distributions.

In this study, we test the impact of four different hypothetical distribution types (Fig. 1).

Ice nucleation propensities observed for individual particle types (*e.g.*, mineral dust) may vary by up to one or two orders of magnitude at a fixed temperature,[5,17] and we represent this behavior by a generalized extreme value (GEV) distribution ($w = 0.3$, $\xi = -0.1$) and a lognormal distribution ($\sigma = 1.2$). GEV distributions are used to evaluate the impact of tails within a J_{het} distribution (*i.e.*, rare, highly ice-active particles).[29] We also
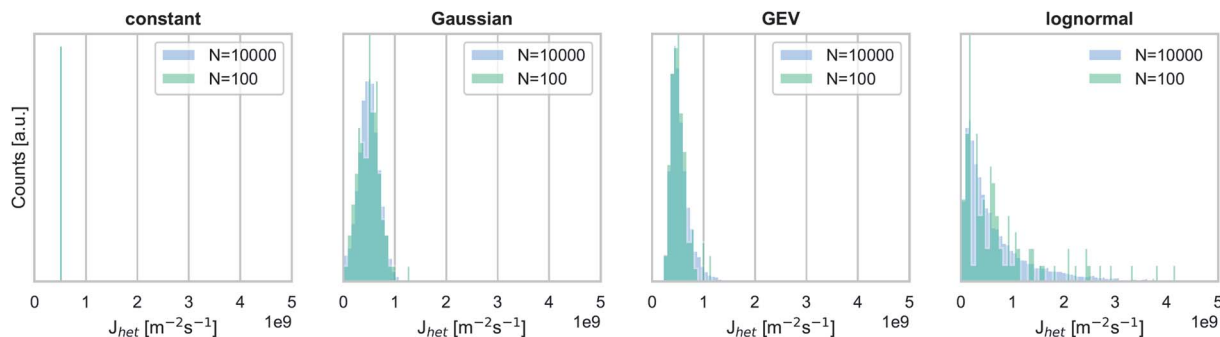
Fig. 1   Nucleation rate coefficient distribution types (median: $J_{het} = 5 \times 10^8$ m^{-2} s^{-1}) used for synthetic experiments shown in Fig. 3 and 4.

employ a broad lognormal distribution to analyze the impact of highly ice-active particles in a population where most individual particles have a low ice nucleation propensity. Note, however, that even our very broad lognormal distribution may still be an underestimate of variability observed for ambient particles with complex mixing states and a wide range of ice nucleation propensities. For example, INP populations consisting of internal and external mixtures of dust, sea spray, and biological particles, each with dramatically different ice nucleation propensities, have been observed at locations around the world. Also, while there is some indication from observations that ice nucleation propensities vary widely across different particle types (*e.g.*, primary biological particles and mineral dust), there are currently no direct measurements of this variability of J_{het} across the same particle class.

As a contrast to these broad distributions, we also include a relatively narrow Gaussian ($\sigma = 0.4$, with σ normalized to the median) and a constant J_{het} value in our analysis. We hypothesize that the skewness of the J_{het} distribution as well as the distribution width are key factors in determining not only the median of simulated f_{ice} values but also the range of possible outcomes.

In addition to analyzing the role of different J_{het} distribution types, we also investigate the impact of ice nucleation efficiencies by analyzing two different median values for each distribution type, namely $J_{het} = 5 \times 10^8$ m^{-2} s^{-1} and $J_{het} = 5 \times 10^{10}$

m^{-2} s^{-1}. These two J_{het} values can also be interpreted as proxies for the ice nucleation propensities of mineral dust particles at two different temperatures (248 K, and 238 K, respectively).[16]

2.3   Simulated aerosol surface distributions

To account for the variability in aerosol surface area, we use two lognormal aerosol size distributions with the same median value ($A = 10^{-12}$ m^2) but with a variable width. As represented in Fig. 2, we specifically analyze a distribution with a width $\sigma = 3.0$, which is more representative of a realistic aerosol distribution in experiments, and a quasi-monodisperse distribution with $\sigma = 1.1$, which is more representative of size-selected experiments.[28]

3   Results and discussion

Fig. 3 shows the range of simulated frozen fractions (f_{ice}) for our Monte Carlo simulations investigating the interplay between J_{het} and aerosol surface area variability. The results shown in Fig. 3 assume a median ice nucleation rate coefficient of $J_{het} = 5 \times 10^8$ m^{-2} s^{-1}, which can be interpreted as a representation of freezing for mineral dusts at 248 K.[17] Fig. 3 shows that the number of droplets or droplet equivalents, *e.g.*, water-filled wells in droplet assays, has a significant impact on the range of possible outcomes and therefore the stochastic uncertainties.
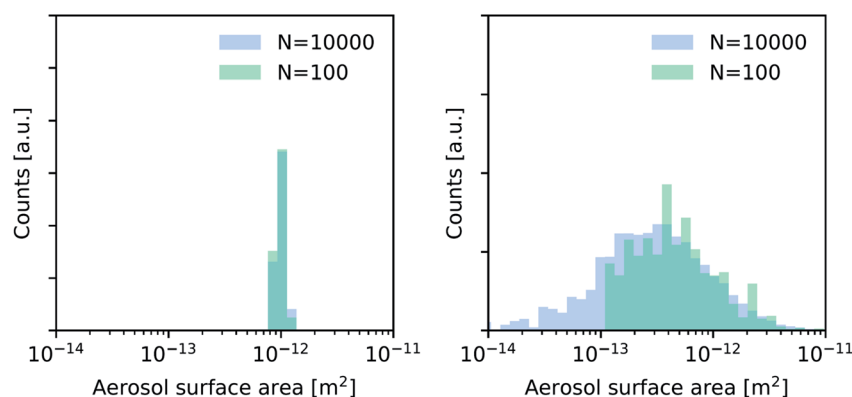

Fig. 2   Exemplary aerosol surface area distributions used for synthetic experiments shown in Fig. 3 and 4—quasi-monodisperse (left) and broad lognormal distribution (right).
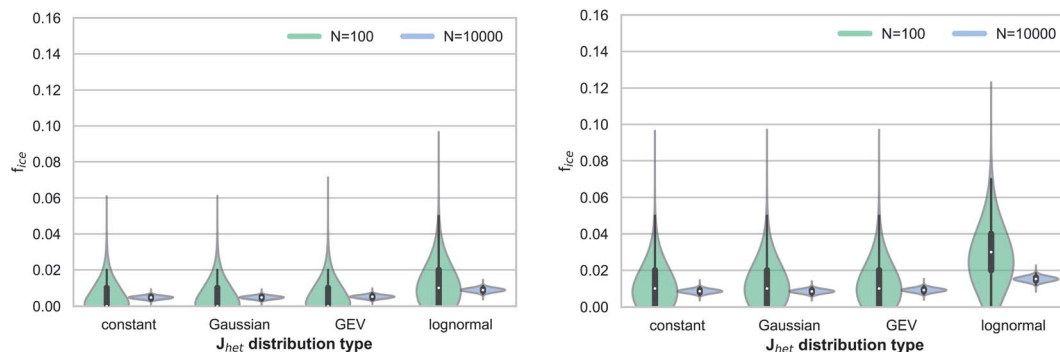
Fig. 3 Violin plots showing the distribution of simulated frozen fractions f_{ice} for median $J_{het} = 5 \times 10^8$ m^{-2} s^{-1} (corresponding to the freezing efficiency of dust at 248 K). Left: results for a quasi-monodisperse ($\sigma = 1.1$) aerosol surface area distribution; right: results for a broad ($\sigma = 3.0$) aerosol surface area distribution (boxplots inside the violins represent median values and quartile ranges).

Additionally, the larger widths of the underlying J_{het} distributions broaden the range of possible outcomes by up to a factor of two for the small droplet ensemble ($N_{drop} = 100$) if all outliers are taken into consideration. This behavior is more pronounced for the quasi-monodisperse aerosol surface area distribution.

In addition to affecting the range of possible outcomes, the variability in J_{het} (*i.e.*, the distribution type) also affects the median value of f_{ice}, particularly for the case of a lognormal distribution. For both aerosol surface area distributions, the median f_{ice} value is shifted by approximately a factor of up to three when comparing between results for the constant J_{het} value and the lognormal J_{het} distribution. This finding demonstrates that the underlying shape of J_{het} distributions may contribute to systematic uncertainties if a narrow Gaussian distribution is implicitly assumed when evaluating observed frozen fractions. Relative measurement uncertainties $\Delta n_s/n_s$ of up to 40% across different measurement techniques[28] translate into similar uncertainties for $\Delta J_{het}/J_{het}$ if eqn (1) and (2) are used. Therefore, for our simulated cases these measurement uncertainties would be smaller than the systematic uncertainties potentially introduced by the variability in J_{het}. Note that all results presented in this study are within the context of a timescale of $\delta t = 10$ s after which the frozen fractions are evaluated in our simulations.

Fig. 4 shows results analogous to Fig. 3 but for a higher median J_{het} value ($J_{het} = 5 \times 10^{10}$ m^{-2} s^{-1}), which can be interpreted as a proxy for immersion freezing of mineral dust particles at temperatures around 238 K.[17] We observe a similar interplay between J_{het} variability and the aerosol surface area distributions, as in Fig. 3 for the quasi-monodisperse surface area. However, the overall sensitivity to the shape of the J_{het} distribution is less pronounced at higher J_{het} values due to the sublinear relationship between frozen fractions f_{ice} and J_{het}.

The relative shift of the median f_{ice} values when comparing between a constant J_{het} value and lognormal J_{het} distribution is slightly smaller, but still in the same range as typical measurement uncertainties. For the broader surface area distribution, we do not observe a consistent relationship between different J_{het} distributions and frozen fractions (*i.e.*, a shift of median f_{ice} values). In both cases (Fig. 3 and 4), we find that the range of possible outcomes (within a confidence interval CI 95%, *i.e.*, the 2.5th and 97.5th percentiles) is similar to estimates using an approximation based on a normal distribution of errors,[30] with more significant deviations in the case of smaller droplet ensembles and for constant J_{het} values (Table 1). This approximation is commonly used to evaluate
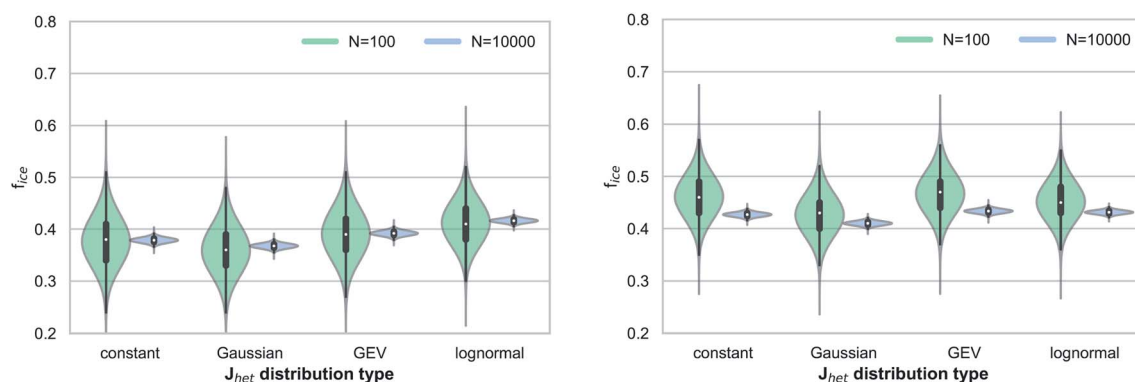

Fig. 4 Violin plots showing the distribution of simulated frozen fractions f_{ice} for median $J_{het} = 5 \times 10^{10}$ m^{-2} s^{-1} (corresponding to the freezing efficiency of dust at 238 K). Left: Results for a quasi-monodisperse ($\sigma = 1.1$) aerosol surface area distribution; right: results for a broad ($\sigma = 3.0$) aerosol surface area distribution.

Table 1 Summary of results shown in Fig. 3 and 4. 2.5th and 97.5th percentile ranges of Monte Carlo simulations (left) compared against estimated confidence intervals (CI 95%) assuming binomial sampling (Agresti and Coull, 1998)—shown are values for the constant value and the lognormal J_{het} distribution

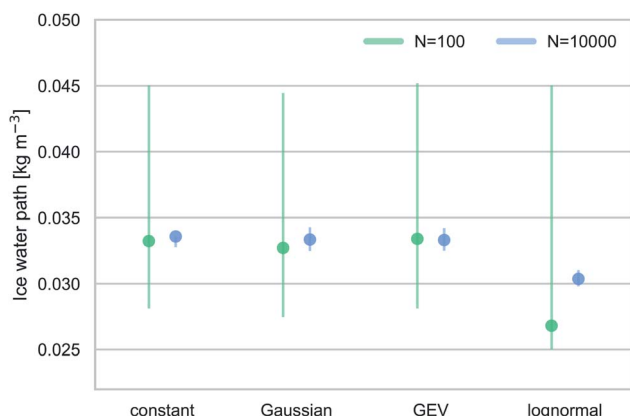|	Constant J_{het} value		Lognormal J_{het} distribution	
	f_{ice}	f_{ice}	f_{ice}	f_{ice}
Experiment type	2.5th perc./CI 95%	97.5th perc./CI 95%	2.5th perc./CI 95%	97.5th perc./CI 95%
Quasi-monodisperse aerosol + low J_{het} ($N = 100$)	0.000/0.001	0.020/0.046	0.000/0.002	0.030/0.053
Polydisperse aerosol + low J_{het} ($N = 100$)	0.000/0.002	0.030/0.054	0.000/0.005	0.050/0.067
Quasi-monodisperse aerosol + high J_{het} ($N = 100$)	0.290/0.297	0.480/0.485	0.330/0.321	0.500/0.511
Polydisperse aerosol + high J_{het} ($N = 100$)	0.380/0.365	0.540/0.557	0.390/0.369	0.540/0.561
Quasi-monodisperse aerosol + low J_{het} ($N = 10\,000$)	0.003/0.004	0.007/0.007	0.006/0.007	0.010/0.010
Polydisperse aerosol + low J_{het} ($N = 10\,000$)	0.007/0.007	0.010/0.011	0.012/0.012	0.016/0.017
Quasi-monodisperse aerosol + high J_{het} ($N = 10\,000$)	0.370/0.369	0.388/0.389	0.407/0.406	0.423/0.425
Polydisperse aerosol + high J_{het} ($N = 10\,000$)	0.424/0.423	0.440/0.442	0.429/0.427	0.444/0.446

Fig. 5 Ice water path estimated based on simulated frozen fractions and the IWP parameterization given in Hawker et al., (2021)—filled markers represent median IWP values and whiskers represent the 5th and 95th percentile.

confidence ranges associated with droplet freezing experiments.[31] Another method of approximation relies on Poisson distributions, implicitly assuming large droplet ensembles and thus not fully resolving statistical uncertainties as a function of sample size.[32]

In conclusion, our simulations demonstrate that the variability in J_{het} may introduce differences in observed frozen fractions, which could lead to systematic uncertainties for parameterizations that are derived from these measurements if the variability in J_{het} is not well known. However, it is unclear how grave consequent errors would be if these parameterizations were used in climate models. To illustrate these effects, we quantify the cloud impacts associated with different J_{het} distributions, and consequently hypothetical INP parameterizations that can be derived from our simulated frozen fractions. Hawker et al. showed that choosing a weaker/stronger temperature dependence of INP parameterizations produced increases/decreases in outgoing radiation, the average cloud fraction and the ice water path (IWP) for deep convective clouds simulated by a cloud resolving model.[33] We combine

our frozen fraction simulations with the relationships reported by Hawker et al.[33] to estimate the impact on modeled clouds.

Fig. 5 shows estimated IWP values, based on frozen fractions simulated for different J_{het} distributions and applying the relationship between $d\log_{10}(\text{INP})/dT$ and IWP given in Hawker et al.[33] for a system of tropical convective clouds. The ranges in Fig. 5 indicate the 5th and 95th percentile of simulated frozen fractions. For the small droplet ensembles, we assume the lower limit to be $q_5(f_{ice}) = 0.001$, except in the case of the lognormal J_{het} distribution where $q_5(f_{ice}) > 0.001$. We use $A = 10^{-12}$ m^2 to convert frozen fractions into n_s values, and then use the same aerosol surface area concentration as in Hawker et al.,[33] $A_{amb} = 5 \times 10^{-5}$ m^2 m^{-3}, to calculate INP concentrations.

Median IWP values are similar for small and large droplet ensembles. The IWPs for the lognormal J_{het} distribution are roughly 25% lower compared to the other three cases. Despite these differences, the estimated IWP values agree within their respective uncertainties, and the impact from assuming different J_{het} distributions or errors in J_{het} within the uncertainties are small.

4 Conclusions

Our synthetic experiments demonstrate that J_{het} distributions may have an impact on observed frozen fractions but only for distributions spanning at least one order of magnitude, and that this impact is more significant at low frozen fractions (i.e., warmer temperatures and less efficient INPs). Very broad aerosol surface area distributions may contribute to a shift in observed frozen fractions by up to a factor of two in our simulation setup, particularly for low frozen fractions. At higher frozen fractions and with a broad aerosol surface area distribution, simulations with different underlying J_{het} distributions cannot be clearly distinguished from each other in our synthetic freezing experiments.

We also infer potential cloud impacts associated with hypothetical ice nucleation parameterizations based on our simulations. The temperature dependence of different ice nucleation parameterizations—which is determined by ice

© 2022 The Author(s). Published by the Royal Society of Chemistry

Environ. Sci.: Atmos., 2022, **2**, 1101–1107 | **1105**

nucleation propensities particularly at warm temperatures and by our ability to measure them—may have an impact on simulated cloud properties, *e.g.*, the IWP in tropical convective cloud systems.[33] For the cases that we considered in this study, these differences appear to be negligible in comparison to order-of-magnitude changes in ambient INP number concentrations.[34] However, for a more comprehensive understanding of these effects, more detailed studies taking into account different cloud types and detailed cloud microphysics are needed.

Our synthetic experiments have shown that the number of freezing droplets has a significant impact on our ability to measure ice nucleation efficiencies with small uncertainty ranges, which agrees with findings by Alpert and Knopf.[22] Note, however, that our synthetic experiments only consider the statistical uncertainties, without taking into consideration other factors that introduce additional uncertainties in real experiments, *e.g.*, the counting efficiency of optical particle counters used to quantify the number of ice crystals or differences in sample handling impacting the comparability of observed frozen fractions across experimental setups.

Our analysis highlights the importance of studies with large droplet ensemble sizes to enhance our ability to precisely measure (median) ice nucleation propensities. These conditions may not be achievable for field measurements seeking to characterize ambient ice nucleating particles because of low number concentrations and highly complex compositions (*i.e.*, numerous ice nucleating components) but can be more easily achieved in laboratory experiments and offline ice nucleation analyses. Also, even for the INP types that have been studied extensively, *e.g.*, mineral dusts, the particle-to-particle variability of J_{het} remains virtually unknown. Finally, we note that effects are expected to be larger in particle populations containing particle types with dramatically different ice nucleation propensities, *e.g.*, internal and external mixtures of sea spray and dust.

Author contributions

IS and SMB designed the study and wrote the paper. IS developed the numerical Monte Carlo tools, with contributions from SMB. IS conducted all analyses.

Conflicts of interest

There are no conflicts to declare.

Acknowledgements

References

1 O. Boucher, D. Randall, P. Artaxo, C. Bretherton, G. Feingold, P. Forster, V.-M. Kerminen, Y. Kondo, H. Liao and U. Lohmann, *et al.*, in *Climate Change 2013: the Physical Science Basis. Contribution of Working Group I to the Fifth Assessment Report of the Intergovernmental Panel on Climate Change*, ed. T. F. Stocker, D. Qin, G.-K. Plattner, M. Tignor, S. K. Allen, J. Boschung, A. Nauels, Y. Xia, V. Bex and P. M. Midgley, Cambridge University Press, 2013, pp. 571–657.

2 J. Mülmenstädt, M. Salzmann, J. E. Kay, M. D. Zelinka, P.-L. Ma, C. Nam, J. Kretzschmar, S. Hörnig and J. Quaas, *Nat. Clim. Change*, 2021, **11**, 508–513.

3 G. Cesana and T. Storelvmo, *J. Geophys. Res., D: Atmos.*, 2017, **122**, 4594–4599.

4 I. Tan, T. Storelvmo and M. D. Zelinka, *Science*, 2016, **352**, 224–227.

5 Z. A. Kanji, L. A. Ladino, H. Wex, Y. Boose, M. Burkert-Kohn, D. J. Cziczo and M. Krämer, *Meteorol. Monogr.*, 2017, **58**, 1.1–1.33.

6 B. J. Murray, K. S. Carslaw and P. R. Field, *Atmos. Chem. Phys.*, 2021, **21**, 665–679.

7 A. Korolev and T. Leisner, *Atmos. Chem. Phys.*, 2020, **20**, 11767–11797.

8 J. Fan, Y. Wang, D. Rosenfeld and X. Liu, *J. Atmos. Sci.*, 2016, **73**, 4221–4252.

9 S. M. Burrows, C. S. McCluskey, G. Cornwell, I. Steinke, K. Zhang, B. Zhao, M. Zawadowicz, A. Raman, G. Kulkarni, S. China, A. Zelenyuk and P. J. DeMott, *Rev. Geophys.*, 2022, **60**, e2021RG000745.

10 L. B. Hande and C. Hoose, *Atmos. Chem. Phys.*, 2017, **17**, 14105–14118.

11 D. Barahona, *Geophys. Res. Lett.*, 2020, **47**, e2019GL086033.

12 J. Savre and A. M. L. Ekman, *J. Geophys. Res.*, 2015, **120**, 4937–4961.

13 S. L. Broadley, B. J. Murray, R. J. Herbert, J. D. Atkinson, S. Dobbie, T. L. Malkin, E. Condliffe and L. Neve, *Atmos. Chem. Phys.*, 2012, **12**, 287–307.

14 C. Marcolli, S. Gedamke, T. Peter and B. Zobrist, *Atmos. Chem. Phys.*, 2007, 5081–5091.

15 I. Steinke, C. Hoose, O. Möhler, P. Connolly and T. Leisner, *Atmos. Chem. Phys.*, 2015, **15**, 3703–3717.

16 B. J. Murray, D. O'Sullivan, J. D. Atkinson and M. E. Webb, *Chem. Soc. Rev.*, 2012, **41**, 6519–6554.

17 C. Hoose and O. Möhler, *Atmos. Chem. Phys.*, 2012, **12**, 9817–9854.

18 D. Niedermeier, R. A. Shaw, S. Hartmann, H. Wex, T. Clauss, J. Voigtländer and F. Stratmann, *Atmos. Chem. Phys.*, 2011, **11**, 8767–8775.

19 L. Ickes, A. Welti and U. Lohmann, *Atmos. Chem. Phys.*, 2017, **17**, 1713–1739.

20 R. J. Herbert, B. J. Murray, T. F. Whale, S. J. Dobbie and J. D. Atkinson, *Atmos. Chem. Phys.*, 2014, **14**, 8501–8520.

21 T. P. Wright and M. D. Petters, *J. Geophys. Res.*, 2013, **118**, 3731–3743.

22 P. A. Alpert and D. A. Knopf, *Atmos. Chem. Phys.*, 2016, **16**, 2083–2107.

23 H. R. Pruppacher and J. D. Klett, *Microphysics of Clouds and Precipitation*, Springer, Dordrecht, 2010.

24 J. Heintzenberg, *Aerosol Sci. Technol.*, 1994, **21**, 46–48.

25 H. J. Bae and J. H. Oh, *Asia-Pacific J. Atmos. Sci.*, 2017, **53**, 403–410.

26 S. J. O'Shea, J. Crosier, J. Dorsey, W. Schledewitz, I. Crawford, S. Borrmann, R. Cotton and A. Bansemer, *Atmos. Meas. Tech.*, 2019, **12**, 3067–3079.

27 S. M. Miller, R. Commane, J. R. Melton, A. E. Andrews, J. Benmergui, E. J. Dlugokencky, G. Janssens-Maenhout, A. M. Michalak, C. Sweeney and D. E. J. Worthy, *Biogeosciences*, 2016, **13**, 1329–1339.

28 N. Hiranuma, S. Augustin-Bauditz, H. Bingemer, C. Budke, J. Curtius, A. Danielczok, K. Diehl, K. Dreischmeier, M. Ebert, F. Frank, N. Hoffmann, K. Kandler, A. Kiselev, T. Koop, T. Leisner, O. Möhler, B. Nillius, A. Peckhaus, D. Rose, S. Weinbruch, H. Wex, Y. Boose, P. J. DeMott, J. D. Hader, T. C. J. Hill, Z. A. Kanji, G. Kulkarni, E. J. T. Levin, C. S. McCluskey, M. Murakami, B. J. Murray, D. Niedermeier, M. D. Petters, D. O'Sullivan, A. Saito, G. P. Schill, T. Tajiri, M. A. Tolbert, A. Welti, T. F. Whale, T. P. Wright and K. Yamashita, *Atmos. Chem. Phys.*, 2015, **15**, 2489–2518.

29 R. P. Sear, *Atmos. Chem. Phys.*, 2013, **13**, 7215–7223.

30 A. Agresti and B. A. Coull, *Am. Stat.*, 1998, **52**, 119–126.

31 T. C. J. Hill, P. J. DeMott, Y. Tobo, J. Fröhlich-Nowoisky, B. F. Moffett, G. D. Franc and S. M. Kreidenweis, *Atmos. Chem. Phys.*, 2016, **16**, 7195–7211.

32 G. Vali, *Atmos. Meas. Tech.*, 2019, **12**, 1219–1231.

33 R. E. Hawker, A. K. Miltenberger, J. M. Wilkinson, A. A. Hill, B. J. Shipway, Z. Cui, R. J. Cotton, K. S. Carslaw, P. R. Field and B. J. Murray, *Atmos. Chem. Phys.*, 2021, **21**, 5439–5461.

34 J. Fan, L. R. Leung, D. Rosenfeld and P. J. DeMott, *Atmos. Chem. Phys.*, 2017, **17**, 1017–1035.

© 2022 The Author(s). Published by the Royal Society of Chemistry

Environ. Sci.: Atmos., 2022, **2**, 1101–1107 | **1107**